Chemistry – A European Journal

ChemEurJ Chemistry Europe European Chemical Societies Publishing

RESEARCH ARTICLE

Surficial N^+ Charge Density as Key Factor for Inhibition of *Pseudomonas* Biofilm Formation in Non-Leaching Quaternary Ammonium-Modified Polydimethylsiloxane Coatings

Paola Marzullo[1,2] | Alessandro Presentato[1] | Vincenzo Campisciano[1] | Enrico Tornatore[1] | Rosa Alduina[1,2] | Francesca D'Anna[1,2] | Francesco Giacalone[1] | Michelangelo Gruttadauria[1,2]

[1]Department of Biological, Chemical and Pharmaceutical Sciences and Technologies (STEBICEF), University of Palermo, Palermo, Italy | [2]Sustainable Mobility Center (Centro Nazionale per La Mobilità Sostenibile—CNMS), Milano, Italy

Correspondence: Michelangelo Gruttadauria (michelangelo.gruttadauria@unipa.it)

Received: 5 October 2025 | **Revised:** 5 January 2026 | **Accepted:** 19 January 2026

Keywords: antibiofilm activity | non-leaching materials | PDMS-based materials | pseudomonas strain | quaternary-ammonium salts | surficial charge density

ABSTRACT

Marine biofouling represents significant environmental and economic concerns, highlighting the need for sustainable and non-leaching antifouling materials. In this work, we developed cross-linked polydimethylsiloxane (PDMS) coatings functionalized with methyldimethoxysilanes bearing quaternary ammonium groups and alkyl side chains of two different lengths (C8 and C12). ^{29}Si and ^{13}C solid-state nuclear magnetic resonance (CP-MAS NMR) and Fourier-transform infrared spectroscopy (FTIR) confirmed the successful incorporation of silanes into the polymer matrix. Surface analysis was carried out by fluorescein assay, surface roughness, and contact angle measurements. Antifouling assays against *Pseudomonas delhiensis* PS27, a robust Gram-negative strain exhibiting strong resilience to environmental stresses, demonstrated notable biofilm inhibition in coatings with higher charge surface density without affecting the physiological fitness of planktonic cells. An observed minimum effective value of surface charge density $(6.23 \pm 0.76)\cdot10^{16}$ N^+/cm^2 for biofilm inhibition was observed. These findings suggest a link between surficial N^+ charge density and antifouling efficacy. The developed coatings represent a promising and durable strategy for environmentally friendly fouling prevention in marine and aquatic environments.

1 | Introduction

Biofilms represent a major concern in both clinical and industrial settings due to their complex architecture, primarily characterized by a self-produced extracellular matrix that encases microbial cells. This matrix confers enhanced protection against conventional antimicrobial agents, contributing to the persistence of infections and treatment failures [1]. Biofilms are responsible for significant economic burdens across diverse industries, including marine, construction, and food processing, primarily through surface contamination, material degradation, and equipment fouling [2–4].

In particular, marine biofouling, characterized by the accumulation of microorganisms, algae, and invertebrates on submerged surfaces, represents a critical issue for maritime industries. It contributes to increased hydrodynamic drag on ships, leading to higher fuel consumption and greenhouse gas emissions, while also accelerating the degradation of materials and structures such as hulls, propellers, offshore platforms, and aquaculture

equipment. Moreover, biofouling can facilitate the spread of invasive species and disrupt local ecosystems, raising significant environmental concerns in addition to economic costs [5].

Traditionally, antifouling strategies in marine environments have relied on coatings composed of soluble or insoluble polymeric matrices, often incorporating biocidal agents such as copper or organotin compounds (e.g., tributyltin), which are gradually released into the surrounding seawater to prevent the settlement of marine organisms. However, concerns over the environmental persistence and toxicity of these compounds, particularly after the global ban of tributyltin by the International Maritime Organization (IMO) in 2008, have driven the search for more sustainable solutions [6, 7].

One promising direction involves the development of hydrophilic, non-fouling surfaces that can form a tightly bound hydration layer through hydrogen bonding or electrostatic interactions [8–10].

Alternatively, fouling-release strategies employ superhydrophobic materials (contact angle value > 150°) that combine microstructured surfaces with inherently low surface energy, often inspired by the lotus leaf effect [11, 12]. The well-established correlation between surface energy and biofouling levels, illustrated by the "Baier curve", shows that lower surface energies generally lead to reduced biofouling accumulation [13]. These materials rely on weak interfacial interactions, allowing organisms to detach more easily under the hydrodynamic shear forces generated during vessel movement. Among the various fouling-release approaches, slippery liquid-infused porous surfaces (SLIPs) represent a new frontier [14, 15].

In the pursuit of environmentally friendly materials that offer sustained antimicrobial performance without leaching biocides into the environment, there is growing interest in contact-active antifouling strategies. These approaches involve the immobilization of antimicrobial agents directly on the material surface, thus compromising the microbial fitness upon contact rather than through diffusion [16]. Commonly employed biocidal components are quaternary ammonium salts (QASs), first described in the 1930s [17] and known for their strong antimicrobial efficacy [18–21].

In our recent work, we provided a comprehensive review of QASs and their applications in antibiofilm strategies, with particular emphasis on their integration into systems for marine environments and water treatment technologies [22]. An effective strategy is to combine the contact-killing action of QASs with the fouling-release properties of polydimethylsiloxane (PDMS)-based materials to achieve greater coating durability. The PDMS surface hardly allows the attachment of microorganisms and dirt, and, as a result, the active surface stays clean and biocides remain effective for longer periods. Moreover, the high flexibility of the PDMS matrix allows the surface exposure of QAS groups.

The antifouling activity of PDMS-QASs composite coatings, using statistically driven experimental approaches, was studied by evaluating key parameters, including the QAS alkyl chain length, its concentration, and PDMS molecular weight. The resulting films demonstrated enhanced seawater stability and strong antibiofilm activity against the marine bacterium *Cellulophaga lytica* and the alga *Navicula incerta* [23]. The same authors also reported the synthesis of QAS-based PDMS materials using methyltriacetoxysilane as a crosslinker, silanol-terminated PDMS of varying molecular weights, and QAS-functionalized trimethoxysilanes with different alkyl chain lengths (C1, C14, and C18). Their study revealed a correlation between surface roughness and hydrophobicity: higher roughness values were observed in films containing higher concentrations of long-chain silanes, which also resulted in increased water contact angles [24]. Additionally, the use of Sum Frequency Generation vibrational spectroscopy enabled the authors to investigate the molecular structure of the polymer surface in contact with water. This analysis focused on how surface organization is influenced by variations in the alkyl chain length, the spacer between the ammonium group and the PDMS backbone, and the type of silane used (trimethoxysilane *vs.* triethoxysilane) [25, 26].

Other authors have focused their attention on the effects of alkyl chain length and quaternary ammonium charge density [27–30].

Quaternary ammonium compounds with short alkyl chains and high grafting density were equally effective against *E. coli* compared to surfaces having long alkyl chains with low grafting density [31].

Over the years, evidence of a strict correlation between antibacterial capacity and surficial N^+ charge density of QAS has been reported, with, in some cases, the determination of threshold values [30, 32–34]. For instance, the lower limit of the QAS surface content required to achieve antibacterial activity for *E. coli* and *S. aureus* is 10^{14} N^+/cm^2 [35–37]; for *E. coli*, the threshold value could be $5{\cdot}10^{15}$ N^+/cm^2 depending on the growth stage of the cells [31].

In this study, we developed novel hybrid coatings composed of cross-linked PDMS films functionalized with QAS-based methyldimethoxysilanes bearing side chains of different lengths (C8 and C12). For each type of QAS-based silane, various weight percentages were incorporated into the PDMS matrix and thoroughly investigated.

The films were characterized by solid-state ^{13}C and ^{29}Si CP-MAS NMR and FTIR spectroscopy to confirm successful crosslinking. Furthermore, surface properties including contact angle, roughness, and the surface exposure of quaternary ammonium groups were analysed, revealing a clear dependence on both the type and concentration of the QAS-based silane used.

Antifouling performance was evaluated against the Gram-negative *Pseudomonas delhiensis* PS27 strain, noted for its high resilience to environmental stresses and robust biofilm formation [38–40]. A correlation emerged between surface characteristics and biofilm prevention efficacy: coatings containing a higher N^+ surface charge density showed greater antibiofilm activity.

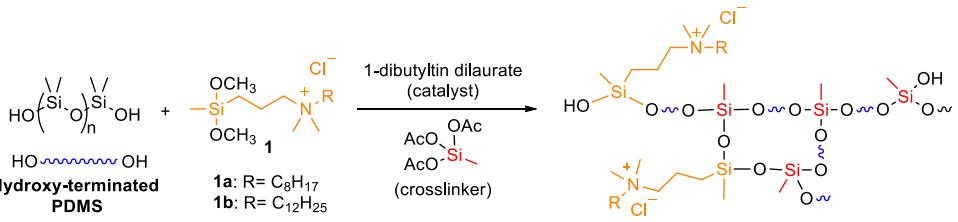

SCHEME 1 | Preparation of cross-linked PDMS/QAS-based silane 1 composite films.

TABLE 1 | Cross-linked polydimethylsiloxane films functionalized with the biocide silane 1a-b[a].

Entry	Sample name	1a (mg)	1b (mg)
1	PDMS@1a.1	100	—
2	PDMS@1a.2	50	—
3	PDMS@1a.3	25	—
4	PDMS@1a.4[b]	100	—
5	PDMS@1a.5[b]	50	–
6	PDMS@1a.6[b]	25	—
7	PDMS@1b.1	—	100
8	PDMS@1b.2	—	50
9	PDMS@1b.3	—	25

[a]Films were prepared using hydroxy-terminated PDMS (1 g), methyltriacetoxysilane (133 μL), 1-dibutyl dilaurate (40 μL), and silanes 1a-b (see Table 1).

[b]Films analogue of entries 1–3 synthesized in the presence of 1 mL of MeOH, used to solubilize the silane 1a.

2 | Results and Discussion

2.1 | Preparation and Characterization of Polydimethylsiloxane Films Grafted with Antibacterial Silane

Here, the quaternary ammonium-based silane **1a** and **1b** (**Scheme 1**), whose synthesis and antibacterial activity were reported in our previous paper [41] have been considered for the design of cross-linked polydimethylsiloxane films exploitable as novel antifouling materials with non-leaching biocidal moieties.

The hydroxy-terminated polydimethylsiloxane (PDMS—cst 700–800) was cross-linked in the presence of the silanes **1** using methyltriacetoxysilane and 1-dibutyltin dilaurate as the cross-linking agent and catalyst, respectively (**Scheme 1**). The cross-linked films were obtained by pouring the polymeric mixture into a petri dish and drying it in an oven at 50°C for 24 h.

Table 1 shows all prepared films with the corresponding weight composition with respect to PDMS and biocidal QAS-based silane.

The resulting polydimethylsiloxane films were characterized by ^{29}Si and ^{13}C CP-MAS NMR spectroscopy (Figure 1). The ^{29}Si CP-MAS NMR spectrum of PDMS crosslinked with methyltriacetoxysilane (**PDMS@**) was overlapped with that of crosslinked PDMS functionalized with biocidal silanes **1a** and **1b** at different weight percentages (**PDMS@1a.1-6** and **PDMS@1b.1-3**) (Figures 1a,b).

The successful cross-linking can be indicated by the peak at approximately −67 ppm assigned to the T^3 system ($RSi(OSi)_3$) [42]. By normalizing all spectra to the intensity of this peak, it was possible to observe for **PDMS@1a.1-3** films an increase in the intensity of the peak relative to D^2 systems ($R_2Si(OSi)_2$) [42] in a manner dependent on the silane concentration (Figure **1a**). This result is consistent with increased silane **1a**/PDMS cross-linking.

Furthermore, the ^{29}Si CP-MAS NMR spectra revealed enhanced silane grafting efficiency onto the PDMS matrix in solvent-free films. Specifically, when comparing the **PDMS@1a.1–3** samples to **PDMS@1a.4–6**, a higher intensity ratio between D^2-type and T^3-type peaks was observed in the former group. The presence of additional cross-linking points for **PDMS@1** films is also confirmed by the disappearance of the peak at ca. −57 ppm, characteristic of the T^2 system ($RSi(OSi)_2OH$) and thus of the free silanol groups [43].

In contrast, the ^{29}Si CP-MAS NMR spectra of films **PDMS@1b** did not display a consistent increase in the intensity of the D^2 signal ($R_2Si(OSi)_2$) with increasing silane concentration (Figure **1b**).

This deviation may be explained by the longer alkyl chain of silane **1b**, which, at higher weight concentrations (10 wt%) in the **PDMS@1b.1** film, likely introduces increased steric hindrance leading to incomplete condensation. As a result, the condensation reaction is hindered, limiting the formation of D^2-type structures in favour of uncondensed D^1 moieties. Further supporting this hypothesis, the **PDMS@1b.1** film, differently from other films, exhibits a D^1 signal ($RSi(CH_3)(OR)OH$) at ca. −15 ppm, indicating the presence of unreacted hydroxyl groups from the silane precursor (Figure **1b**).

In the ^{13}C CP-MAS NMR spectra of **PDMS@1a** and **PDMS@1b** films (Figure **2a**,**b**), peaks of methyl bonded to silicon atoms of PDMS (at ca. 1.44 ppm) and cross-linker (at ca. −2 ppm) can be observed [44]. Carbons of cross-linked biocidal silane **1a** or **1b** resonate in the region between 13 ppm and 52 ppm, confirming the successful functionalization. The signal with the highest chemical shift (at ca. 52 ppm) can be assigned to the positive nitrogen-bonded methyl. The normalization of all spectra to the intensity of the peak at about 1.44 ppm allowed the following considerations to be made. The more intense signals between 13 and

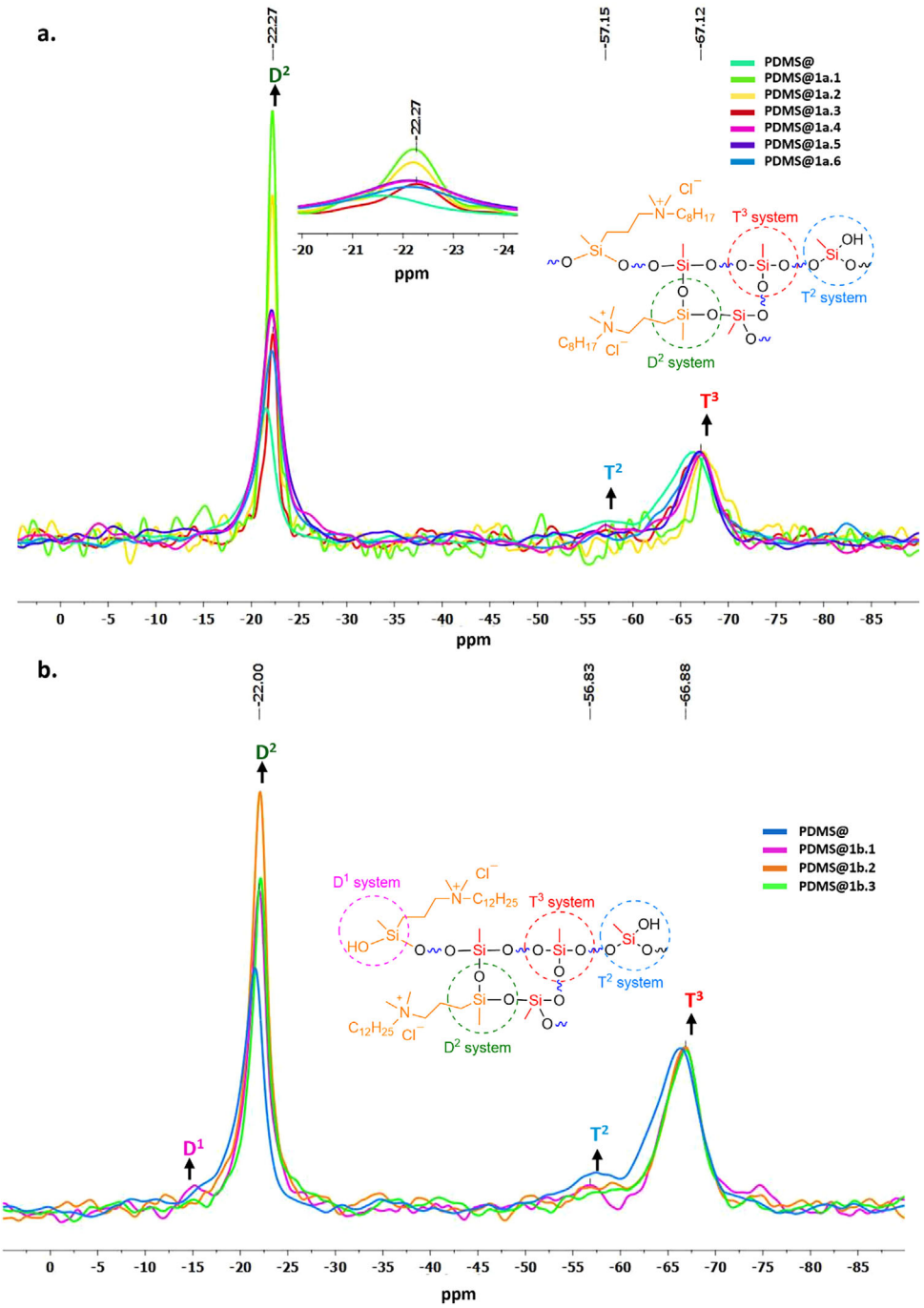

FIGURE 1 | ^{29}Si CP-MAS NMR spectra of cross-linked **PDMS@1a** (a) and **PDMS@1b** (b) films with different weight percentages of silane **1a** and **1b**.

52 ppm for **PDMS@1a.1** (Figure 2a) and **PDMS@1b.1** (Figure 2b) films reflect a higher weight percentage of QAS-based silane. In contrast, overlapped spectra show an opposite trend for the signal intensity related to the methyl cross-linker at ca −2 ppm, which is more intense in the pristine PDMS film (**PDMS@**). This suggests that silanes **1a** and **1b** may substitute the cross-linker in specific regions.

The FTIR spectra shown in Figure 3 exhibit prominent stretching bands corresponding to siloxane (Si—O—Si) groups, observed at 801 cm^{-1} and in the 1020–1098 cm^{-1} range. The successful functionalization of the **PDMS@1a.1** and **PDMS@1b.1** films is here confirmed by the appearance of characteristic vibrational bands associated with C—H stretching at 2858 cm^{-1} and C—H bending at 1420 cm^{-1}, which are indicative of alkyl chains adjacent to the positively charged nitrogen atoms of the quaternary ammonium silanes.[4] Notably, the spectra of QAS-functionalized films exhibit a broad absorption band near 3400 cm^{-1}, attributed to the presence of physically adsorbed water molecules interacting with the quaternary ammonium groups on the surface.

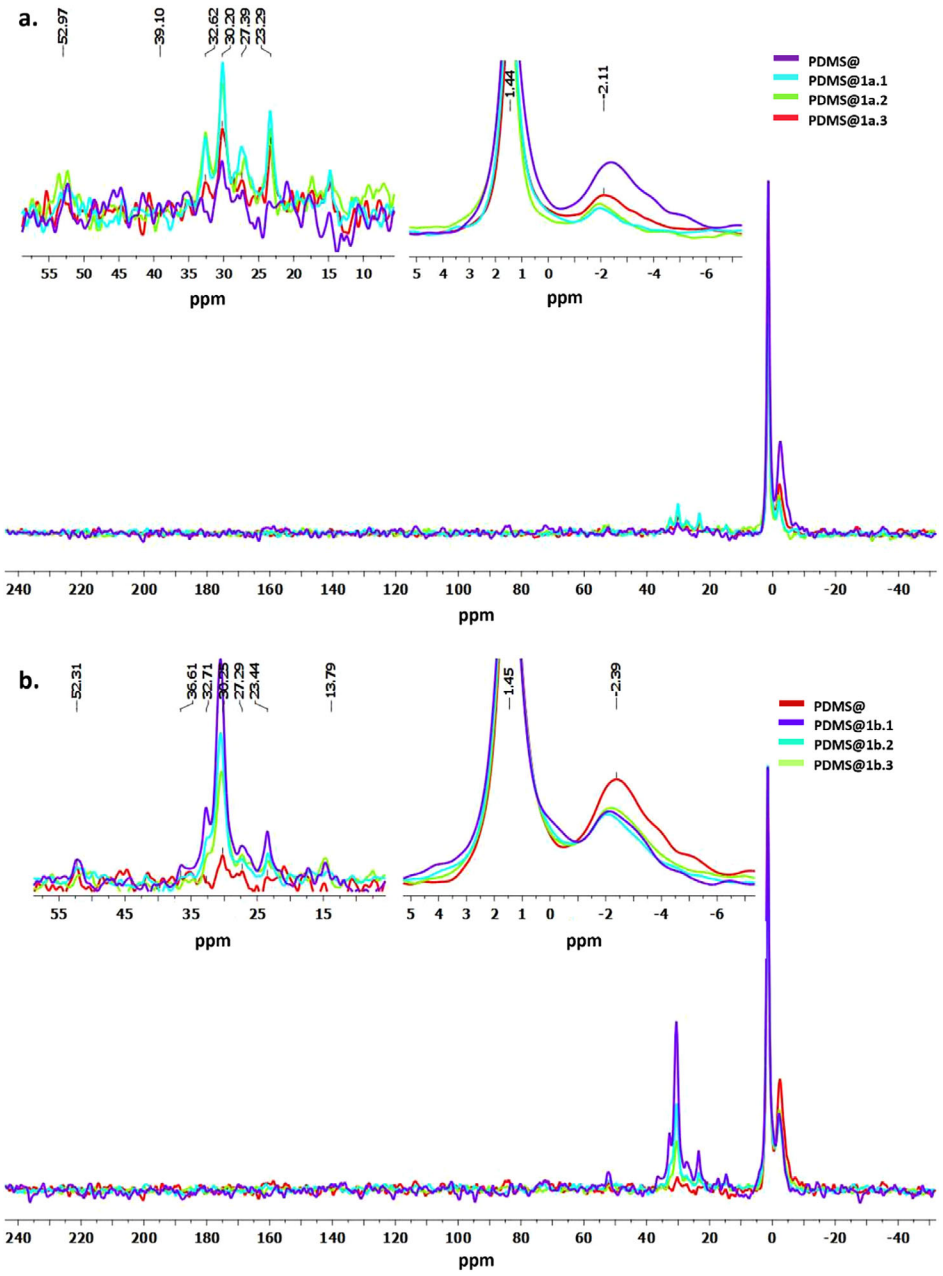

FIGURE 2 | ^{13}C CP-MAS NMR spectra of cross-linked **PDMS@1a** (a) and **PDMS@1b** (b) films with different weight percentages of silane **1a** and **1b**.

2.2 | Surface Analysis of PDMS/QAS-Based Silane Composite Films

2.2.1 | Fluorescein Assay

The surface charge density of the QAS-modified films was assessed by a fluorescein assay following the established protocol [45]. This assay measured the specific binding of fluorescein to surface-exposed quaternary ammonium groups, with the absorbance of the desorbed dye quantified at 501 nm (Figure 4 **a,b**).

To correct for nonspecific binding, the absorbance measured on a control PDMS film was subtracted. The corrected surface charge density values are presented in Table **2**.

Importantly, as the weight percentage of the quaternary ammonium silane **1a** and **1b**, used for functionalization, increases, there is a statistically significant rise in surface-exposed ammonium group density (Table 2>**, entries 1 and 4**).

2.2.2 | Analysis of Surface Roughness by Optical Profilometer

Given the subsequent evaluation of antibiofilm activity, we first assessed the surface roughness, as it is well known that increased roughness can lead to enhanced micro- and nano-structuring, which may improve the antifouling properties of surfaces [46, 47].

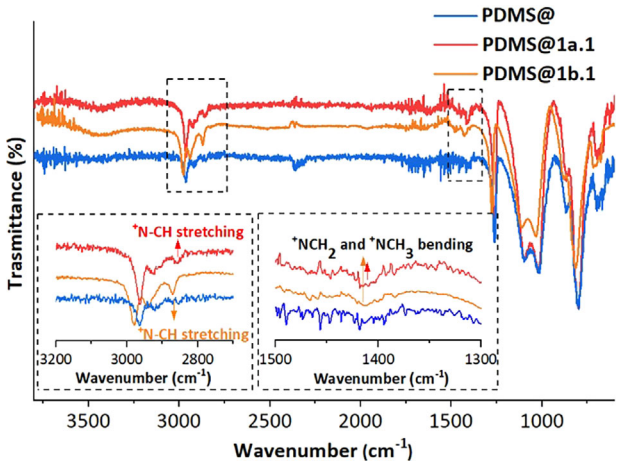

FIGURE 3 | FTIR spectra of PDMS@1a.1 and PDMS@1b.1 films overlapped with those of the pristine PDMS@ film.

TABLE 2 | Surface charge density of PDMS films prepared with different weight percentages of biocidal silane **1a** or **1b**.

Entry	Sample name	1a or 1b (wt%) with respect to PDMS	Charge density (N^+/cm^2)
1	**PDMS@1a.1**	10	$(1.37 \pm 0.09) \cdot 10^{17}$ *; **[a]
2	PDMS@1a.2	5	((2.77 ± 0.70) . 1016
3	PDMS@1a.3	2.5	(6.61 ± 0.46) . 1015
4	PDMS@1b.1	10	((3.93 ± 0.62) . 1017** a
5	PDMS@1b.2	5	(6.23 ± 0.76) . 1016
6	PDMS@1b.3	2.5	(3.70 ± 0.19) . 1016

[a]* *p value* < 0.05 as compared to PDMS@1a.2; ** *p value* < 0.005 as compared to PDMS@1a.3; ** *p value* < 0.005 as compared to PDMS@1b.2 and PDMS@1b.3.

The analysis of the surface characteristics of the **PDMS@1** films was carried out through 2D (Figure 5a) and 3D optical profilometry images (Figure **5b**) acquisition. The 3D surface profile is characterized by recessed areas highlighted in blue/purple and elevated regions in red/yellow.

Figure 5c reports the measured R_a value (R_a = arithmetic mean deviation of the evaluated profile), which indicates the amplitude of the surface roughness over the sample length.

Films containing a higher percentage of silane **1a** and **1b**, namely **PDMS@1a.1** and **PDMS@1b.1**, exhibit significantly higher surface roughness than those of the pristine **PDMS** film and of samples with lower silane content (**PDMS@1a.3** and **PDMS@1b.3**).

As shown in Figure 5b, the **PDMS@1a.1** film exhibits more pronounced height variations (±200 μm) compared to the **PDMS@1b.1** film (±100 μm). However, the corresponding average roughness (R_a) values reported in Figure 5c show an opposite trend, with **PDMS@1b.1** displaying a higher R_a value. This apparent contradiction can be explained by considering that R_a does not directly reflect the visual roughness of a surface, but rather the frequency and intensity of height deviations from the mean level. In other words, a surface with smaller but more frequent variations can yield a higher R_a value [48, 49]. In the case of the **PDMS@1a.1** sample, the peaks and valleys are likely more isolated and symmetrically distributed, which reduces their overall contribution to R_a. Conversely, although the 3D optical profile of the **PDMS@1b.1** sample appears visually smoother, it may possess a finer texture composed of high-frequency, low-amplitude microroughness, which contributes to an increased R_a value. The presence of D^1 structure in **PDMS@1b.1**, absent in **PDMS@1a.1**, could also play a role in the texture of the film.

Finally, the **PDMS@1a.3** and **PDMS@1b.3** films, which contain a lower concentration of silane, exhibited significantly reduced R_a values compared to both the 10% silane-loaded samples (**PDMS@1a.1** and **PDMS@1b.1**) and the unmodified **PDMS@**.

2.2.3 | Contact Angle Measurements

The contact angle is significantly affected by various factors, such as the type of functional silane, its concentration, and how it is distributed within the polymer matrix. To investigate the wetting properties of the functionalized PDMS surfaces, we measured both the static contact angle at time zero (T_0) and the dynamic contact angle after one minute (T_1), allowing us to evaluate temporal changes in surface wettability.

Representative droplet profiles at time T_0 for the **PDMS@1a** and **PDMS@1b** are shown in Figure 6 **a,b**, while the corresponding quantitative data are reported in Figure 6c.

Obtained results can be interpreted considering that the overall architecture of PDMS films is governed by the hydrophobic nature of the silane used and the PDMS/silane ratio. Since mixing occurs in a solvent-free environment, the resulting molecular organization reflects a balance between the hydrophobic effects of both components. In these films, alkyl chains of the silane are arranged with varying degrees of exposure, directly influencing the surface charge density.

Although the exposure of alkyl chains and ammonium groups dictates the surface charge density, the silane concentration simultaneously modulates the surface roughness.

Our findings confirm that surface topography plays a more dominant role than charge density in determining the contact angle, in full agreement with Wenzel's model [50]. According to this model, the increase in surface roughness induced by higher silane concentrations (10 and 5 wt%) in the **PDMS@1a.1-2** and **PDMS@1b.1** films amplifies the intrinsic hydrophobicity of the matrix. This morphological effect effectively counterbalances the hydrophilicity of the charged groups, maintaining a contact angle that is nearly constant and comparable to that of pristine **PDMS@** (Figure 6 **a–c**) [24]. In contrast, the reduction in the static contact angle (T0) observed for **PDMS@1a.3** and the lower dynamic value (T1) for **PDMS@1b.3** are attributable to their

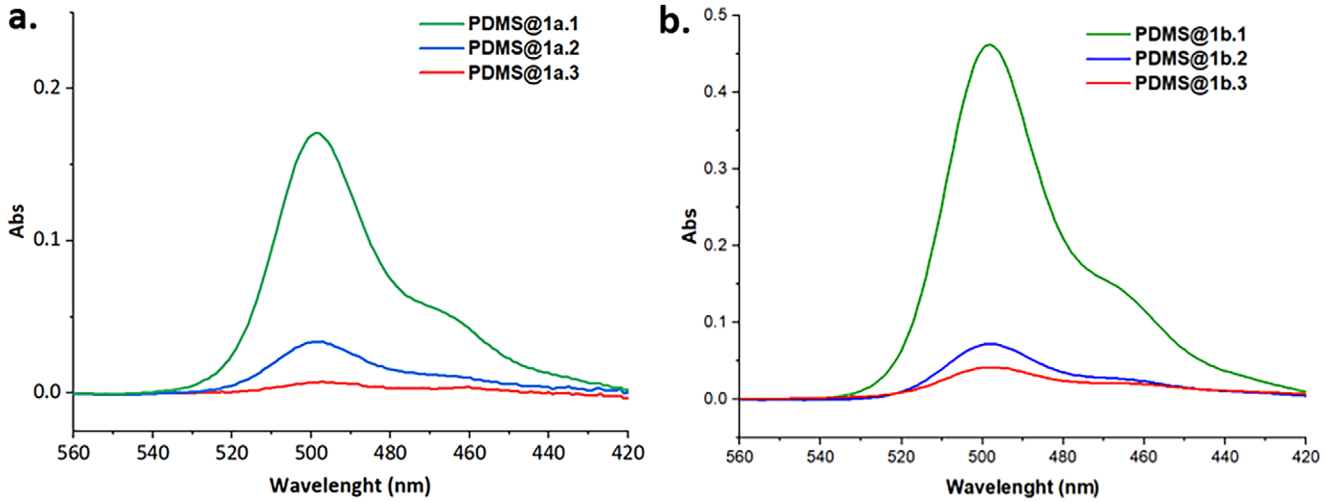

FIGURE 4 | Representative UV-Visible spectra of solution obtained by desorbing the fluorescein bound to the quaternary ammonium moieties on the surface of PDMS@1a (a) and PDMS@1b (b) films.

smoother surface profiles (Figure 6a, **panel D and** Figure 6c). In these low-silane concentration samples (2.5 wt%), the reduced roughness is no longer able to compensate for the presence of hydrophilic groups leading to a decrease in water repellence. This result may suggest also a different surface arrangement of hydrophilic ammonium groups at lower silane concentrations. Finally, it is noted that the **PDMS@1b** series exhibits slightly higher average contact angles than the **PDMS@1a** counterpart, while following the same dependency on surface roughness.

2.3 | Antibiofilm Activity of PDMS-Composite Films

The development of new antifouling materials increasingly focuses on environmentally safe compounds that incorporate covalently bound biocidal functionalities. In a previous study conducted by our group, we demonstrated that silanes **1a** and **1b** exhibit noteworthy antibacterial properties. Furthermore, PDMS-based nanocomposite films containing silica gel grafted with silane **1a** showed promising antifouling performance [41].

Building on these findings, the PDMS–silane composite films developed here emerged as strong candidates for evaluating antibiofilm properties. The biological activity was assessed against the *P. delhiensis* PS27 strain, an environmental isolate belonging to a genus comprising microbial species featuring a natural opportunistic behaviour and strong ability to form biofilms [39].

As shown in Figure 7a, the in vitro assay revealed that the pristine PDMS film significantly reduced biofilm formation compared to the uncoated control surface. This behaviour is likely attributed to the inherent hydrophobicity of the PDMS matrix. Notably, the antifouling performance was further enhanced through the covalent incorporation of biocidal silanes. The results indicate that the antifouling efficacy is dependent on the concentration of the quaternary ammonium-based silane. A significant outcome was observed for **PDMS@1a.1** film, which completely inhibited bacterial adhesion at a 10 wt% loading of silane **1a** (Figure 7a), while no inhibition of adhesion was observed in the other two materials, **PDMS@1a.2** and **PDMS@1a.3**.

As evidenced by previously reported characterization techniques, the **PDMS@1a.1** film displays hydrophobic behaviour, resulting from the combined effects of silane alkyl chains, a high surface density of ammonium groups, and increased surface roughness, being factors that collectively contribute to its enhanced antifouling performance.

PDMS@1b films, functionalized with silane **1b**, exhibited outstanding antifouling performance, achieving complete inhibition of fouling at concentrations of 10 wt% (**PDMS@1b.1**) and even at 5 wt% (**PDMS@1b.2**) (Figure 7a).

Importantly, the antifouling activity of **PDMS@1a.1** and **PDMS@1b.1** films did not negatively impact the physiological fitness of planktonically growing *Pseudomonas* cells with microbial titres statistically comparable to those of unmodified PDMS and the positive control (Figure 7b). These results confirm that the biocidal moieties are covalently immobilized within the polymeric matrix, with no detectable release into the surrounding medium. In contrast, PDMS films synthesized in the presence of 1 mL of methanol (PDMS@1a.4–6), used as a solubilising agent for silane **1a**, showed evidence of biocide release. This phenomenon correlates with an increase in concentration-dependent toxicity towards planktonic cells, particularly observed in the **PDMS@1a.4** film, which exhibited a higher silane **1a** content (Figure 7b). The release of biocide was further confirmed by experiments in deuterated water (D_2O) followed by ^1H NMR analysis (Figure 8), where the spectrum of the D_2O in contact with sample **PDMS@1a.4** showed signals corresponding to protons of the QAS-based biocidal silane **1a**. This experimental evidence is in agreement with the fact that the presence of methanol as solvent hampers the condensation of dimethoxymethylsilane **1a** in the structure of the PDMS film. As consequence, the PDMS film also contains not-covalently linked silane that is released.

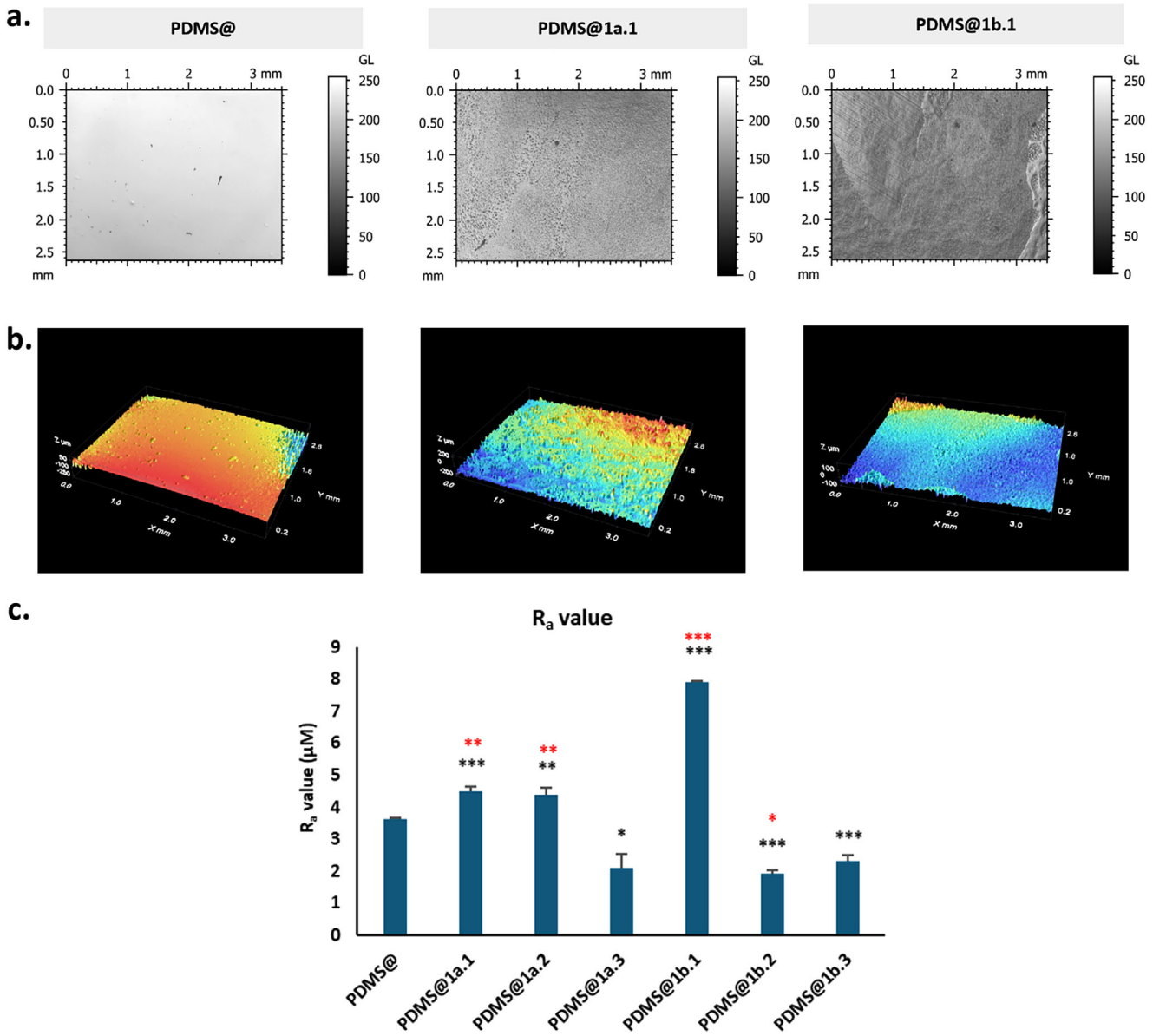

FIGURE 5 | Representative 2D (a) and 3D optical profile (b) of roughness for PDMS@, PDMS@1a.1 and PDMS@1b.1 films; (c) Average surface roughness (Ra) values of PDMS films functionalized with different concentrations of silane. Black asterisks: * *p value* < 0.05, ** *p value* < 0.005 and *** *p value* < 0.0005 as compared to PDMS@; Red asterisks: ** *p value* < 0.005 and *** *p value* < 0.0005 as compared to PDMS@1a.3 and PDMS@1b.3, respectively. Data are presented as mean ± standard deviation from measurements taken at three points on each sample.

3 | Experimental Section

All solvents and reagents were obtained from commercial sources and were used without purification. Methyltriacetoxysilane and PDMS hydroxy-terminated (cst. 700–800) were purchased from Fluorochem (Hadfield, UK); 1-dibutyltin dilaurate was purchased from TCI (Zwijndrecht, Belgium); fluorescein sodium salt and cetyltrimethylammonium bromide (CTAB) were purchased from Sigma Aldrich (Burlington, MA, US).

^{29}Si Cross-Polarization Magic Angle Spinning (CP-MAS) NMR spectra were acquired on a Bruker (Billerica, MA, US) Advance II 400 MHz (9.4 T) spectrometer operating at 79.5 MHz with a MAS rate of 6 kHz, a 90° pulse on 1H of 5.1 µs, a delay time of 2s, and a contact time of 8 ms. ^{13}C Cross Polarization Magic Angle Spinning (CP-MAS) NMR spectra were acquired on a Bruker (Billerica, MA, US) Advance II 400 MHz (9.4 T) spectrometer operating at 100.6 MHz with a MAS rate of 6 kHz, a delay time of 3 s, and a contact time of 2 ms. The Hartman–Hahn condition was optimized using adamantane as the standard.

3.1 | Preparation of Polydimethylsiloxane Films Grafted With QAS-Based Silane

Hydroxy-terminated polydimethylsiloxane (PDMS-OH) (1 g) was mixed with the appropriate amount of quaternary ammonium-based silane (**1a** or **1b**) and stirred at room temperature for

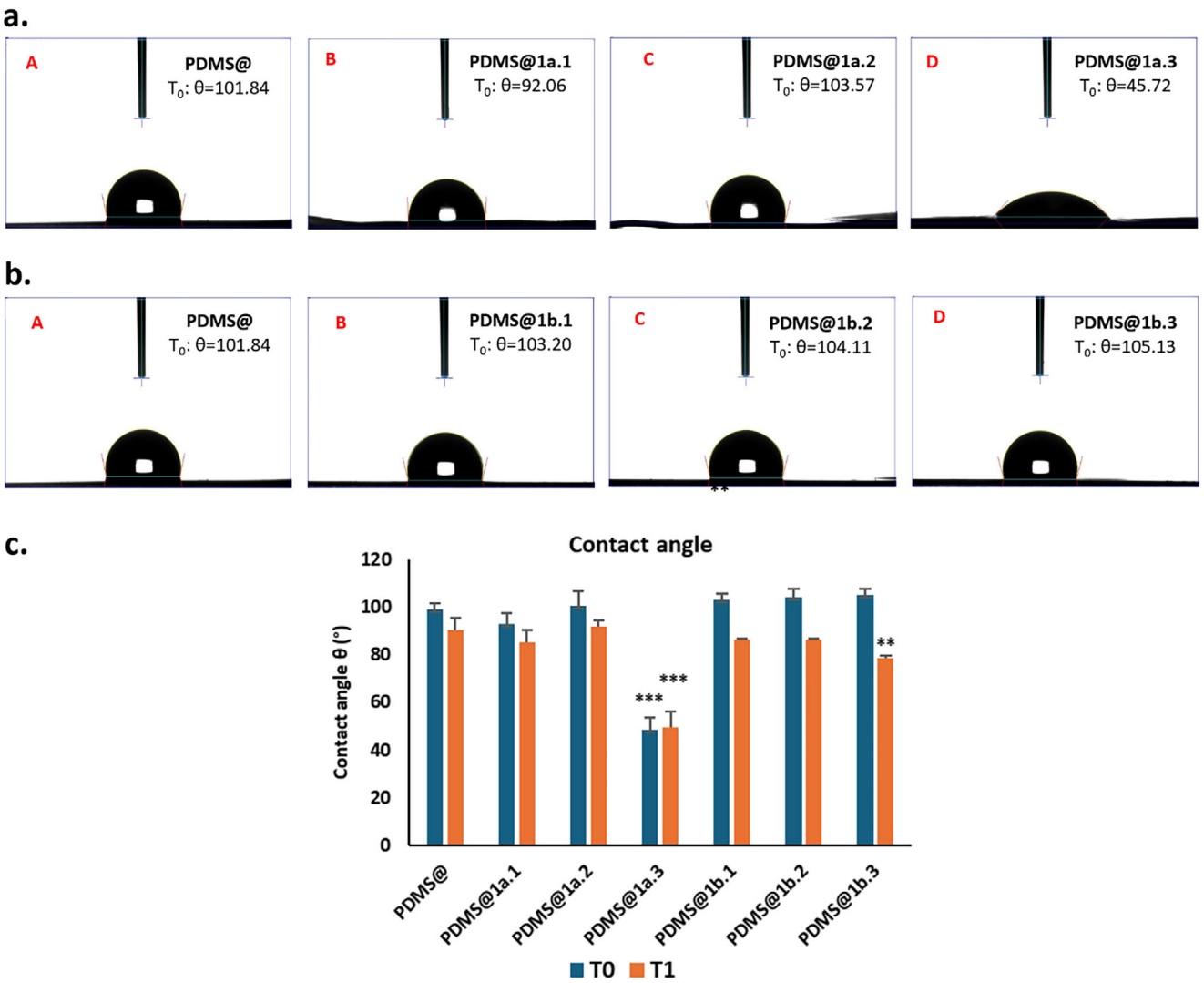

FIGURE 6 | Representative images of static contact angle (T_0) measurements for PDMS films functionalized with increasing weight percentages of silane 1a (a) and silane 1b (b); (c) Static (T_0, blue) and dynamic (T_1, orange) contact angle values for pristine and silane-functionalized PDMS films. Data are presented as mean ± standard deviation from measurements taken at three points on each sample. A statistically significant reduction in T_0 and T_1 contact angle is observed for PDMS@1a.3 compared to PDMS@, PDMS@1a.1 and PDMS@1a.2 (***p *value* < 0.0005). A statistically significant reduction in T_1 contact angle is observed for PDMS@1b.3 compared to PDMS@, PDMS@1b.1 and PDMS@1b.2 (**p *value* < 0.005).

30 min to ensure homogenization. To initiate cross-linking, methyltriacetoxysilane (133 μL) was added, and the mixture was stirred for an additional 15 min at 45°C. Subsequently, 40 μL of dibutyltin dilaurate catalyst was added, and the resulting mixture was immediately poured into a Petri dish. The cross-linking process was completed by curing the films in an oven at 50°C for 24 h.

3.2 | FTIR Spectroscopy

An accurately weighed amount of finely ground solid sample (approximately 1–2 mg) was thoroughly mixed with dry, spectroscopic-grade potassium bromide (KBr) powder (about 100–200 mg) using a mortar and pestle. The resulting homogeneous mixture was then placed into a pellet die and compressed using a hydraulic press (typically applying a pressure of 6–10 tons) to obtain a thin, transparent pellet. The pellet was subsequently mounted in the sample holder of the FTIR spectrometer. Spectra were acquired over the desired wavenumber range (400-4000 cm^{-1}) using a Cary 630 FTIR spectrometer (Agilent Technologies, Santa Clara, CA, USA).

3.3 | Fluorescein Assay

Discs (8 mm in diameter) of the films under investigation were incubated with 3 mL of a 1% (*w*/*v*) fluorescein sodium salt solution for 20 min to facilitate the binding of the dye to ammonium groups present on the film surface. After incubation, the dye solution was removed, and the discs were thoroughly rinsed with distilled water (5 × 2 mL) to eliminate any unbound fluorescein. The films were then immersed in 3 mL of a 0.1% (*w*/*v*) cetyltrimethylammonium bromide (CTAB) solution in distilled water and gently shaken for 2 h to promote desorption of the bound dye. Following this treatment, 0.9 mL of the resulting solution was collected, and its absorbance at 501 nm

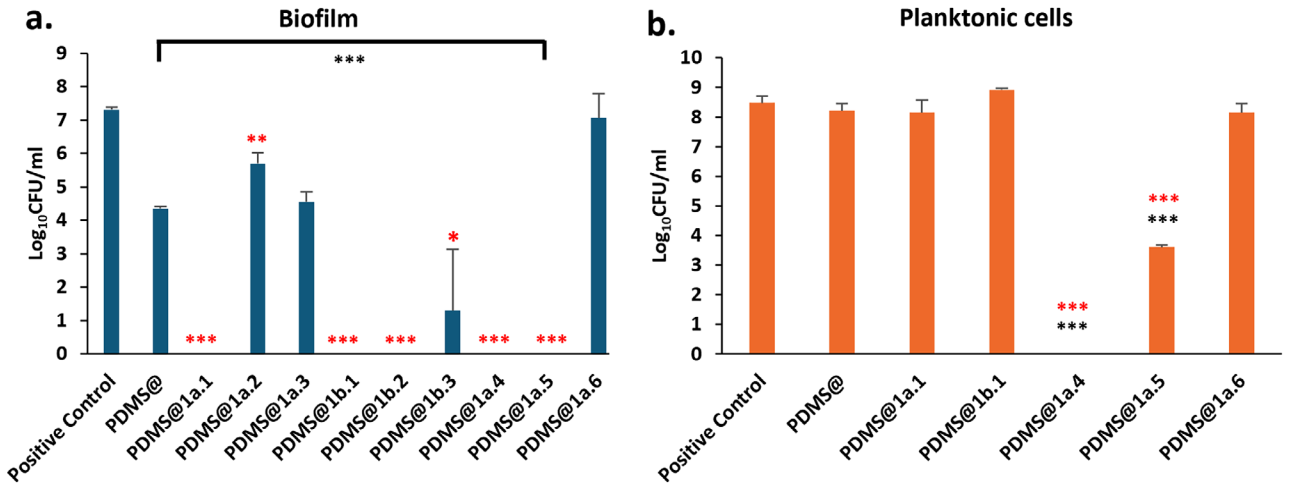

FIGURE 7 | (a) Bar graph illustrating the biofilm inhibition efficacy of PDMS films functionalized with QAS-based silanes against *P. delhiensis* PS27 cells. All tested films, except PDMS@1a.6, showed significant reductions in microbial adhesion compared to the positive control (black asterisks; ***p value < 0.0005). Red asterisks indicate statistical significance when comparing each film to pristine PDMS@ film (***p *value* < 0.0005, **p *value* < 0.005, *p *value* < 0.05). (b) Bar graph showing the microbial counts of planktonic cells exposed to PDMS/QAS-based composite films. Red and black asterisks represent p-values relative to pristine PDMS@ and the positive control, respectively.

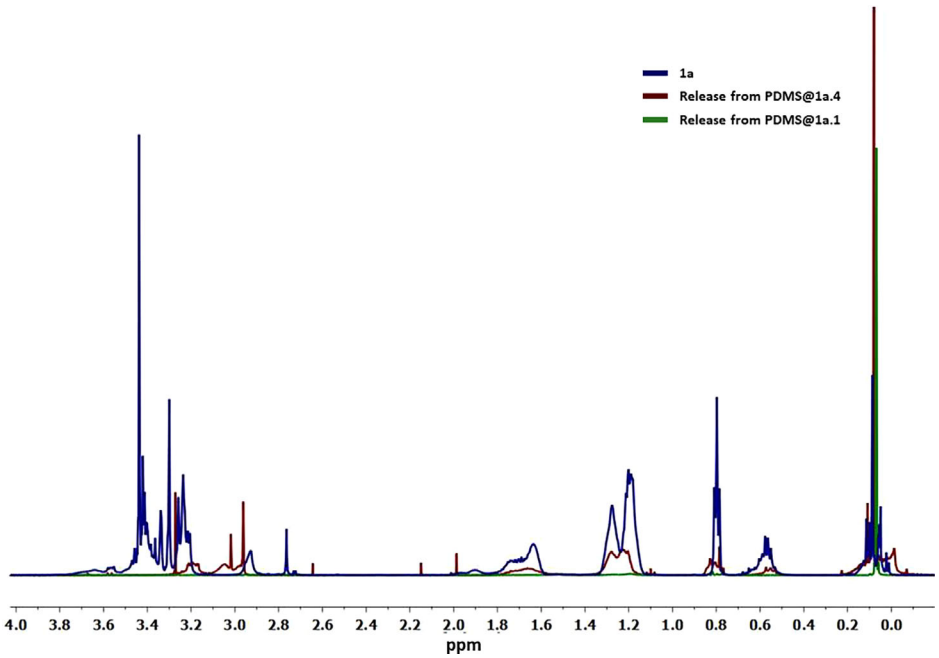

FIGURE 8 | Spectra of deuterated water kept in contact with PDMS@1a.1 (green) and PDMS@1a.4 (red) films overlapped with the ^{1}HNMR spectrum of biocide silane 1a (blue).

was measured after the addition of 10% (w/v) of a 100 mM phosphate buffer (pH 8). The extinction coefficient of fluorescein under these conditions was independently determined to be 67852 $M^{-1}\cdot cm^{-1}$.

3.4 | Contact Angle Measurements

The surface hydrophobicity of the films was evaluated using a video contact angle goniometer (FTA 1000 C Class, First Ten Angstroms, Portsmouth, VA, USA). A droplet of deionized water was carefully deposited onto the film surface, and images were captured immediately (T0) and after 1 min (T1). The contact angles were determined by analysing the droplet shape using dedicated software. Each measurement was performed in triplicate at room temperature, and the results are reported as the mean ± standard deviation

3.5 | Optical Profilometer Analysis

Surface topography was analysed using a Sensofar S Neox 3D optical profilometer (Barcelona, Spain), which enabled high-resolution roughness measurements following ISO 25178 stan-

dards. Before scanning, each film was cleaned using oil-free compressed air to eliminate surface contaminants.

Three-dimensional surface data were acquired using a 10× optical objective and subsequently processed with SensoMAP software to extract metrological parameters. In particular, the R_a value, the arithmetical mean height of the profile, was calculated for each scanned area. Final values for each sample were reported as the average of measurements obtained from multiple surface regions.

3.6 | Biofilm Formation Inhibition Assay

The anti-biofilm efficacy of composite PDMS-based films (namely, **PDMS@1a.1** through **1a.6**, and **PDMS@1b.1** through **1b.3**) against *P. delhiensis* PS27 was evaluated following a previously established protocol [51], with minor modifications. Briefly, *P. delhiensis* cells were precultured by inoculating a single colony into Tryptic Soy Broth (TSB; Merck Life Science S.r.l., Milan, Italy) and incubated at 37°C under orbital shaking (180 rpm) for approximately 16 h. The resulting culture was then diluted to an initial concentration of 1×10^7 CFU mL^{-1} and dispensed into 96-well microtiter plates, each well containing a submerged circular disk of the respective composite film.

Biofilm development was promoted by incubating the cultures at 37°C for 24 h under shaking conditions (180 rpm). Following incubation, planktonic cells were removed and serially diluted in sterile 0.9% (w/v) NaCl solution to determine viable cell counts (reported as CFU per millilitre of culture in logarithmic scale with standard deviation). Simultaneously, the composite film disks were carefully retrieved, washed three times to eliminate loosely adherent bacterial cells, and transferred into 200 μL of sterile saline solution. To dislodge the biofilm-associated biomass, samples were subjected to ultrasonic treatment in a bath sonicator (35 kHz) for 30 min in iced water.

The microbial load within the biofilm was then quantified by serial dilution of the resulting sonicate and subsequent colony enumeration. All experiments were performed in triplicate, and data are expressed as mean log CFU per biofilm ± standard deviation.

4 | Conclusions

In this study, we successfully developed and characterized cross-linked PDMS-based composite films functionalized with quaternary ammonium (QAS)-based silanes, specifically compounds **1a** and **1b**. These materials were designed as non-leaching antifouling surfaces. The covalent incorporation of silanes into the PDMS matrix, confirmed by solid-state CP-MAS NMR and FTIR spectroscopy, enabled the creation of stable networks with tuneable surface properties. Films synthesized under solvent-free conditions demonstrated superior silane grafting efficiency and structural integration compared to those prepared using methanol as a solubilising agent for the QAS precursors.

Surface analysis was carried out by fluorescein binding assays, contact angle and 3D optical profilometry measurements. No significant deviations from the starting contact angle value of pristine PDMS were observed, except for **PDMS@1a.3**, which showed a smoother surface.

PDMS@1a.1 and, especially, **PDMS@1b.1** exhibited high surface roughness and high densities of quaternary ammonium groups, correlating with complete inhibition of *P. delhiensis* PS27 biofilm formation. However, surface roughness cannot be considered alone as a key factor; indeed, **PDMS@1a.2** (5 wt% silane), which showed comparable surface roughness to **PDMS@1a.1**, did not inhibit biofilm formation. On the other hand, **PDMS@1b.2**, which showed much lower surface roughness than **PDMS@1b.1**, completely inhibited biofilm formation.

Surface charge density can be identified as the main parameter that affects antimicrobial activity; yet, the mode of action of antimicrobial polymer surfaces is still under debate, and there is no single explanation for their activity since materials vary so much in their chemical architecture.

Thus, we can conclude that the incorporation of silanes into the PDMS matrix leads to substantial alterations in surface properties, resulting in improved antibiofilm behaviour that could be related to the surface charge density values. Indeed, an observed minimum effective value of surface charge density of $(6.23 \pm 0.76) \cdot 10^{16}$ N^+/cm^2, for no biofilm formation was found. The higher value compared to *E. coli* ($1 \cdot 10^{14}$ N^+/cm^2) can be ascribed to the different nature of the microorganism.

Importantly, no biocidal release was observed from these films, as confirmed by the preserved viability of planktonic cells, indicating that the antimicrobial functionalities remained immobilized within the polymeric matrix. In contrast, films processed with methanol showed evidence of active compound release and associated toxicity, emphasizing the relevance of solvent-free fabrication for safety and material durability.

Throughout biological experiments, no contact-killing effect was observed, suggesting that the exposed quaternary ammonium groups, above the observed minimum effective value of surface charge density, discourage surface colonization. The effectiveness of synthesizing materials where the N^+ surface charge density can be properly modulated could contribute to the development of more efficient coatings with no-contact killing properties.

Overall, the PDMS–QAS composite films represent a promising platform for durable, non-leaching antifouling coatings. Future work will aim to assess their long-term stability and effectiveness in real environmental settings.

Acknowledgments

This research has been partially supported by the European Union—NextGenerationEU—National Sustainable Mobility Center CN00000023, Italian Ministry of University and Research Decree n. 1033—17/06/2022, spoke 3, CUP B73C22000760001. The authors are grateful to Dr. P. Bonomo, Dr. E. Morici, and Dr. A. Spinella of the ATeN Center (University of Palermo) for their expert technical assistance with contact angle, optical profilometry, and NMR measurements, respectively.

Conflicts of Interest

The authors declare no conflicts of interest.

Data Availability Statement

The data that support the findings of this study are available in the supplementary material of this article.

References

1. J. W. Costerton, P. S. Stewart, and E. P. Greenberg, "Bacterial Biofilms: A Common Cause of Persistent Infections," *Science* 284, no. 5418 (1999): 1318–1322, https://doi.org/10.1126/science.284.5418.1318.

2. P. S. Murthy and R. Venkatesan. "Industrial Biofilms and Their Control." In *'Marine and Industrial Biofouling*, edited by H.-C. Flemming, P. S. Murthy, R. Venkatesan and K. Cookse (Berlin, Heidelberg: Springer Berlin Heidelberg, 2009): 65–101, https://doi.org/10.1007/978-3-540-69796-1.

3. G. Shineh, M. Mobaraki, M. J. Perves Bappy, and D. K. Mills, "Biofilm Formation, and Related Impacts on Healthcare, Food Processing, and Packaging, Industrial Manufacturing, Marine Industries, and Sanitation–A Review," *Applied Microbiology* 3 (2023): 629–665, https://doi.org/10.3390/applmicrobiol3030044.

4. M. Cámara, W. Green, C. E. MacPhee, et al., "Economic Significance of Biofilms: A Multidisciplinary and Cross-sectoral Challenge," *npj Biofilms and Microbiomes* 8, no. 1 (2022): 42, https://doi.org/10.1038/s41522-022-00306-y.

5. P. Vuong, A. McKinley, and P. Kaur, "Understanding Biofouling and Contaminant Accretion on Submerged Marine Structures," *npj Materials Degradation* 7, no. 1 (2023): 50, https://doi.org/10.1038/s41529-023-00370-5.

6. A. Kotrikla, "Environmental Management Aspects for TBT Antifouling Wastes from the Shipyards," *Journal of Environmental Management* 90 (2009): S77–S85, https://doi.org/10.1016/j.jenvman.2008.07.017.

7. X. Wang, Q. Jiang, D. Han, et al., "Progress in Anti-Biofouling Materials and Coatings for the Marine Environment," *Journal of Environmental Sciences* 161 (2025): 494–510, https://doi.org/10.1016/j.jes.2025.05.038.

8. D. Li, Q. Wei, C. Wu, et al., "Superhydrophilicity and Strong Salt-affinity: Zwitterionic Polymer Grafted Surfaces with Significant Potentials Particularly in Biological Systems," *Advances in Colloid and Interface Science* 278, (2020) 102141, https://doi.org/10.1016/j.cis.2020.102141.

9. T. Ekblad, G. Bergström, T. Ederth, et al., "Poly(ethylene glycol)-Containing Hydrogel Surfaces for Antifouling Applications in Marine and Freshwater Environments," *Biomacromolecules* 9, no. 10 (2008): 2775–2783, https://doi.org/10.1021/bm800547m.

10. Z. G. Estephan, P. S. Schlenoff, and J. B. Schlenoff, "Zwitteration as an Alternative to PEGylation," *Langmuir* 27, no. 11 (2011): 6794–6800, https://doi.org/10.1021/la200227b.

11. Y. Zhan, S. Yu, A. Amirfazli, A. R. Siddiqui, and W. Li, "Recent Advances in Antibacterial Superhydrophobic Coatings," *Advanced Engineering Materials* 24, no. 4 (2022): 2101053, https://doi.org/10.1002/adem.202101053.

12. P.-Y. Zhu, D.-Q. Feng, M. Yasir, et al., "Enhanced Antifouling Capability of PDMS/Cu2O-anchored Fe-based Amorphous Coatings," *Surface and Coatings Technology* 475 (2023): 130192, https://doi.org/10.1016/j.surfcoat.2023.130192.

13. R. E. Baier, "Surface Behaviour of Biomaterials: The Theta Surface for Biocompatibility," *Journal of Materials Science: Materials in Medicine* 17, no. 11 (2006): 1057–1062, https://doi.org/10.1007/s10856-006-0444-8.

14. X. Liu, X. Gu, Y. Zhou, W. Pan, J. Liu, and J. Song, "Antifouling Slippery Surface Against Marine Biofouling," *Langmuir* 39, no. 38 (2023): 13441–13448, https://doi.org/10.1021/acs.langmuir.3c00986.

15. W. Yao, L. Wu, L. Sun, B. Jiang, and F. Pan, "Recent Developments in Slippery Liquid-infused Porous Surface," *Progress in Organic Coatings* 166 (2022): 106806, https://doi.org/10.1016/j.porgcoat.2022.106806.

16. Q. Su, Y. Xue, C. Wang, et al., "Strategies and Applications of Antibacterial Surface-modified Biomaterials," *Bioactive Materials* 53 (2025): 114–140, https://doi.org/10.1016/j.bioactmat.2025.07.009.

17. G. Domagk, "A New Class of Disinfectants," *Deut Med Wochenschr* 61 (1935): 829–832.

18. P. Elena and K. Miri, "Formation of Contact Active Antimicrobial Surfaces by Covalent Grafting of Quaternary Ammonium Compounds," *Colloids and Surfaces B: Biointerfaces* 169 (2018): 195–205, https://doi.org/10.1016/j.colsurfb.2018.04.065.

19. E. K. Riga, M. Vöhringer, V. T. Widyaya, and K. Lienkamp, "Polymer-Based Surfaces Designed to Reduce Biofilm Formation: From Antimicrobial Polymers to Strategies for Long-Term Applications," *Macromolecular Rapid Communications* 38, no. 20 (2017): 1700216, https://doi.org/10.1002/marc.201700216.

20. G. C. Lainioti and D. Druvari, "Designing Antibacterial-Based Quaternary Ammonium Coatings (Surfaces) or Films for Biomedical Applications: Recent Advances," *International Journal of Molecular Sciences* 25, no. 22 (2024): 12264, https://doi.org/10.3390/ijms252212264.

21. D. Crncevic, L. Krce, Z. Brkljaca, et al., "A Dual Antibacterial Action of Soft Quaternary Ammonium Compounds: Bacteriostatic Effects, Membrane Integrity, and Reduced In Vitro and In Vivo Toxicity," *RSC Advances* 15, no. 2 (2025): 1490–1506, https://doi.org/10.1039/D4RA07975B.

22. P. Marzullo, M. Gruttadauria, and F. D'Anna, "Quaternary Ammonium Salts-Based Materials: A Review on Environmental Toxicity, Anti-Fouling Mechanisms and Applications in Marine and Water Treatment Industries," *Biomolecules* 14, no. 8 (2024): 957, https://doi.org/10.3390/biom14080957.

23. P. Majumdar, E. Lee, N. Patel, S. J. Stafslien, J. Daniels, and B. J. Chisholm, "Development of Environmentally Friendly, Antifouling Coatings Based On Tethered Quaternary Ammonium Salts in a Crosslinked Polydimethylsiloxane Matrix," *Journal of Coatings Technology and Research* 5, no. 4 (2008): 405–417, https://doi.org/10.1007/s11998-008-9098-4.

24. P. Majumdar, E. Lee, N. Patel, et al., "Combinatorial Materials Research Applied to the Development of New Surface Coatings IX: An Investigation of Novel Antifouling/Fouling-release Coatings Containing Quaternary Ammonium Salt Groups," *Biofouling* 24, no. 3 (2008): 185–200, https://doi.org/10.1080/08927010801894660.

25. Y. Liu, C. Leng, B. Chisholm, S. Stafslien, P. Majumdar, and Z. Chen, "Surface Structures of PDMS Incorporated with Quaternary Ammonium Salts Designed for Antibiofouling and Fouling Release Applications," *Langmuir* 29, no. 9 (2013): 2897–2905, https://doi.org/10.1021/la304571u.

26. S. Ye, P. Majumdar, B. Chisholm, S. Stafslien, and Z. Chen, "Antifouling and Antimicrobial Mechanism of Tethered Quaternary Ammonium Salts in a Cross-linked Poly(dimethylsiloxane) Matrix Studied Using Sum Frequency Generation Vibrational Spectroscopy," *Langmuir* 26, no. 21 (2010): 16455–16462, https://doi.org/10.1021/la1001539.

27. H. Zhou, F. Li, M. D. Weir, and H. H. Xu, "Dental Plaque Microcosm Response to Bonding Agents Containing Quaternary Ammonium Methacrylates with Different Chain Lengths and Charge Densities," *Journal of Dentistry* 41, no. 11 (2013): 1122–1131, https://doi.org/10.1016/j.jdent.2013.08.003.

28. D. Gokkaya, M. Topuzogullari, T. Arasoglu, K. Trabzonlu, M. M. Ozmen, and S. Abdurrahmanoğlu, "Antibacterial Properties of Cationic Copolymers as a Function of Pendant Alkyl Chain Length and Degree of Quaternization," *Polymer International* 70, no. 6 (2021): 829–836, https://doi.org/10.1002/pi.6170.

29. L.-H. Yin, B. Ran, T.-J. Hu, C. Yang, J.-J. Fei, and Y.-H. Li, "Preparation of Highly Efficient Antibacterial Polymeric Films via the Modulation of Charge Density and Hydrophobicity," *RSC Advances* 7, no. 10 (2017): 6006–6012, https://doi.org/10.1039/C6RA26071C.

30. H. Zhang, S. Zhao, A. Li, et al., "Structure-dependent Antimicrobial Mechanism of Quaternary Ammonium Resins and a Novel Synthesis of Highly Efficient Antimicrobial Resin," *Science of The Total Environment* 768 (2021): 144450, https://doi.org/10.1016/j.scitotenv.2020.144450.

31. H. Murata, R. R. Koepsel, K. Matyjaszewski, and A. J. Russell, "Permanent, Non-leaching Antibacterial Surfaces—2: How High Density Cationic Surfaces Kill Bacterial Cells," *Biomaterials* 28, no. 32 (2007): 4870–4879, https://doi.org/10.1016/j.biomaterials.2007.06.012.

32. H. Zhang, A. Li, K. Bian, S. Shen, and P. Shi, "Surficial N+ Charge Density Indicating Antibacterial Capacity of Quaternary Ammonium Resins in Water Environment," *PLoS ONE* 15, no. 9 (2020): e0239941, https://doi.org/10.1371/journal.pone.0239941.

33. R. Kügler, O. Bouloussa, and F. Rondelez, "Evidence of a Charge-density Threshold for Optimum Efficiency of Biocidal Cationic Surfaces," *Microbiology (Reading, England)* 151, no. 5 (2005): 1341–1348, https://doi.org/10.1099/mic.0.27526-0.

34. J. Huang, R. R. Koepsel, H. Murata, et al., "Nonleaching Antibacterial Glass Surfaces via "Grafting Onto": The Effect of the Number of Quaternary Ammonium Groups on Biocidal Activity," *Langmuir* 24, no. 13 (2008): 6785–6795, https://doi.org/10.1021/la8003933.

35. Z. Pan, Z. Liu, S. Yang, et al., "Covalent Grafting of Quaternary Ammonium Salt-Containing Polyurethane onto Silicone Substrates to Enhance Bacterial Contact-Killing Ability," *Polymers* 17, no. 1 (2025), https://doi.org/10.3390/polym17010017.

36. Z. Wu, X. Chen, Z. Hao, et al., "Eco-friendly Quaternary Ammonium Modified PDMS Coatings With Integrated Anti-bacterial, Anti-algae, and Marine Anti-fouling Properties," *Surface and Coatings Technology* 509 (2025): 132211, https://doi.org/10.1016/j.surfcoat.2025.132211.

37. R. Kaur and S. Liu, "Antibacterial Surface Design—Contact Kill," *Progress in Surface Science* 91, no. 3 (2016): 136–153, https://doi.org/10.1016/j.progsurf.2016.09.001.

38. F. C. Capri, E. Prazzi, G. Casamento, D. Gambino, G. Cassata, and R. Alduina, "Correlation Between Microbial Community and Hatching Failure in Loggerhead Sea Turtle Caretta Caretta," *Microbial Ecology* 86, no. 3 (2023): 1923–1933, https://doi.org/10.1007/s00248-023-02197-8.

39. K. D. Xu, P. S. Stewart, F. Xia, C. T. Huang, and G. A. McFeters, "Spatial Physiological Heterogeneity in Pseudomonas aeruginosa Biofilm Is Determined by Oxygen Availability," *Applied and Environmental Microbiology* 64, no. 10 (1998): 4035–4039, https://doi.org/10.1128/aem.64.10.4035-4039.1998.

40. A. Presentato, S. Lampis, A. Vantini, et al., "On the Ability of Perfluorohexane Sulfonate (PFHxS) Bioaccumulation by Two Pseudomonas sp. Strains Isolated from PFAS-Contaminated Environmental Matrices," *Microorganisms* 8, no. 1 (2020): 92, https://doi.org/10.3390/microorganisms8010092.

41. P. Marzullo, A. Presentato, F. D'Anna, et al., "A New Synthetic Approach for High Surface Area Mesoporous Silica and Its Use Towards Sustainable Antifouling Materials," *RSC Sustainability* 3, no. 5 (2025): 2352–2365, https://doi.org/10.1039/D5SU00047E.

42. I. S. Protsak, Y. M. Morozov, W. Dong, Z. Le, D. Zhang, and I. M. Henderson, "A 29Si, 1H, and 13C Solid-State NMR Study on the Surface Species of Various Depolymerized Organosiloxanes at Silica Surface," *Nanoscale Research Letters* 14, no. 1 (2019): 160, https://doi.org/10.1186/s11671-019-2982-2.

43. J. Cui, P. Chatterjee, I. I. Slowing, and T. Kobayashi, "In Situ 29Si Solid-state NMR Study of Grafting of Organoalkoxysilanes to Mesoporous Silica Nanoparticles," *Microporous and Mesoporous Materials* 339 (2022): 112019, https://doi.org/10.1016/j.micromeso.2022.112019.

44. S. U. A. Redondo, E. Radovanovic, I. L. Torriani, and I. V. P. Yoshida, "Polycyclic Silicone Membranes. Synthesis, Characterization and Permeability Evaluation," *Polymer* 42, no. 4 (2001): 1319–1327, https://doi.org/10.1016/S0032-3861(00)00520-6.

45. J. C. Tiller, C. J. Liao, K. Lewis, and A. M. Klibanov, "Designing Surfaces That Kill Bacteria on Contact," *Proceedings of the National Academy of Sciences* 98, no. 11 (2001): 5981–5985, https://doi.org/10.1073/pnas.111143098.

46. F. Wan, Q. Ye, and F. Zhou. 2015. "Antifouling of Micro-/Nanostructural Surfaces." In *'Antifouling Surfaces and Materials: From Land to Marine Environment*, edited by F. Zho] (Berlin, Heidelberg: Springer Berlin Heidelberg, 2015): 83–103, https://doi.org/10.1007/978-3-662-45204-2.

47. N. Wang, R. Zhang, K. Liu, et al., "Application of Nanomaterials in Antifouling: A Review," *Nano Materials Science* 6 (2024): 672–700, https://doi.org/10.1016/j.nanoms.2024.01.009.

48. International Organization for Standardization, *Geometrical Product Specifications (GPS) — Surface Texture: Profile Method — Terms, Definitions and Surface Texture Parameters*, ISO 4287: 2009.

49. International Organization for Standardization, Geometrical Product Specifications (GPS) — Surface Texture: Areal, ISO 25178-1:2016.

50. Y. Deng, C. Peng, M. Dai, et al., "Recent Development of Super-wettable Materials and Their Applications in Oil-water Separation," *Journal of Cleaner Production* 266 (2020): 121624, https://doi.org/10.1016/j.jclepro.2020.121624.

51. E. Piacenza, A. Presentato, E. Zonaro, et al., "Antimicrobial Activity of Biogenically Produced Spherical Se-nanomaterials Embedded in Organic Material Against *Pseudomonas aeruginosa* and *Staphylococcus aureus* Strains on Hydroxyapatite-coated Surfaces," *Microbial Biotechnology* 10, no. 4 (2017): 804–818, https://doi.org/10.1111/1751-7915.12700.